Spectrochimica Acta Part A: Molecular and Biomolecular Spectroscopy 134 (2015) 316–325

Contents lists available at ScienceDirect

Spectrochimica Acta Part A: Molecular and Biomolecular Spectroscopy

journal homepage: www.elsevier.com/locate/saa

Vibrational spectroscopic (FT-IR and FT-Raman) studies, HOMO–LUMO, NBO analysis and MEP of 6-methyl-1-({[(2E)-2-methyl-3-phenyl-prop-2-en-1-yl]oxy}methyl)-1,2,3,4-tetra-hydroquinazoline-2,4-dione, a potential chemotherapeutic agent, using density functional methods

Sr.S.H.Roseline Sebastian [a,b], Abdul-Malek S. Al-Tamimi [c], Nasser R. El-Brollosy [d], Ali A. El-Emam [d], C. Yohannan Panicker [e,*], Christian Van Alsenoy [f]

[a] Department of Physics, Karpagam University, Eachanari, Coimbatore, Tamil Nadu, India
[b] Christhu Jyothi Public School, Rajakkad, Idukki, Kerala, India
[c] Department of Pharmaceutical Chemistry, College of Pharmacy, Salman Bin Abdulaziz University, Alkharj 11942, Saudi Arabia
[d] Department of Pharmaceutical Chemistry, College of Pharmacy, King Saud University, Riyadh 11451, Saudi Arabia
[e] Department of Physics, TKM College of Arts and Science, Kollam, Kerala, India
[f] Department of Chemistry, University of Antwerp, B2610 Antwerp, Belgium

HIGHLIGHTS

- IR, Raman spectra and NBO analysis were reported.
- The wavenumbers are calculated theoretically using Gaussian09 software.
- The wavenumbers are assigned using PED analysis.
- The geometrical parameters are in agreement with XRD data.

GRAPHICAL ABSTRACT

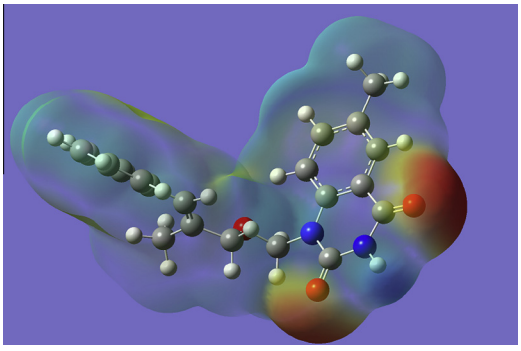

ARTICLE INFO

Article history:
Received 10 April 2014
Received in revised form 19 May 2014
Accepted 3 June 2014
Available online 25 June 2014

Keywords:
Quinazoline
FTIR
FT-Raman
Hyperpolarizability

ABSTRACT

6-Methyl-1-({[(2E)-2-methyl-3-phenyl-prop-2-en-1-yl]oxy}methyl)-1,2,3,4-tetra-hydroquinazoline-2,4-dione was prepared *via* treatment of silylated 6-methylquinazoline-2,4-dione with bis-[(*E*)-2-methyl-3-phenylallyloxy]methane. FT-IR and FT-Raman spectra were recorded and analyzed. The vibrational wavenumbers were computed using DFT methods and are assigned with the help of potential energy distribution method. The first hyperpolarizability, infrared intensities and Raman activities also reported. The geometrical parameters of the title compound obtained from XRD studies are in agreement with the calculated (B3LYP) values. The stability of the molecule arising from hyper-conjugative interaction and charge delocalization has been analyzed using NBO analysis. The HOMO and LUMO analysis are used to determine the charge transfer within the molecule. MEP was performed by the B3LYP method and from the MEP it is evident that the negative charge covers the C=O group and the positive region is over the phenyl ring and NH group.

* Corresponding author. Tel.: +91 9895370968.
E-mail address: cyphyp@rediffmail.com (C. Yohannan Panicker).

http://dx.doi.org/10.1016/j.saa.2014.06.039
1386-1425/

Introduction

Quinazolines and quinazoline-2,4-dione derivatives are important nitrogenous hetero-cycles that have been known for their diverse pharmacological activities. The major chemotherapeutic activities displayed by quinazoline derivatives are the anti-bacteria, anticancer, antiviral and anti-tubercular activities [1–12]. In addition, several quinazoline derivatives were proved to possess potent anticonvulsant [2,13–16] and diuretic [17] activities. Several quinazoline derivatives have been reported for their antibacterial, antifungal, anti-Human Immunodeficiency Virus (HIV) [18], anticonvulsant [19], anti-fibrillatory [20] and diuretic [21] activities. The 2,3-disubstituted quinazolones have been predicted to possess antiviral and antihypertensive activities [22]. Synthesis of vascinone, a naturally occurring bioactive alkaloid having a quinazolone system, has been reported [23]. Alagarsamy et al. [24] have reported the synthesis and analgesic, anti-inflammatory and antibacterial activities of some novel 2-phenyl-3-substituted quinazoline-4(3H)-ones. Costa et al. [25] reported the synthesis of 4H-3,1-benzoxazines, quinazoline-2-ones and quinoline-4-ones. These nitrogen hetero-cycles can be used as valuable intermediates for the preparation of dye stuffs [25] and pharmaceutical products [26–28] since they exhibit a wide range of biological activities. A number of reports have shown that broad classes of 4-anilinoquinazolines are potent and highly selective inhibitors of EGF-R phosphorylation [29,30]. Nanda et al. [31] reported the anti-bacterial activity and QSAR studies of some 3-{arylideneamino}-2-phenyl quinazoline-4(3H)-ones. The three dimensional quantitative structure activity relation (QSAR) studies for one large set of quinazoline type epidermal growth factor receptor (EGF-R) inhibitors were conducted using two types of molecular field analysis techniques: comparative molecular field analysis and comparative molecular similarity indices analysis [32]. In recent years, much effort has been put into the design and synthesis of HIV-1 non-nucleoside reverse transcriptase inhibitors (NNRTIs). El-Brollosy [33] reported the synthesis of a series of quinazoline-2,4(1H,3H)-dione non-nucleoside analogues of the reverse transcriptase inhibitor TNK-651. In the present study, IR and Raman spectrum of 6-methyl-1-({[(2E)-2-methyl-3-phenyl-prop-2-en-1-yl]oxy}methyl)-1,2,3,4-tetrahydroquinazoline-2,4-dione were reported both experimentally and theoretically. The energies, degrees of hybridization, populations of the lone electron pairs of oxygen, energies of their interaction with the anti-bonding orbital of the benzene ring and the electron density distribution and $E(2)$ energies have been calculated by NBO analysis using DFT method to give clear evidence of stabilization originating from the hyper-conjugation of various intra-molecular interactions. There has been growing interest in using organic molecules for nonlinear optical devices, functioning as second harmonic generators, frequency converters, electro-optical modulators, etc., because of the large second order electric susceptibilities of organic materials. Since the second order electric susceptibility is related to first hyperpolarizability, the search for organic chromophores with large first hyperpolarizability is fully justified.

Experimental details

The title compound was prepared *via* treatment of silylated 6-methylquinazoline-2,4-dione with bis-[(*E*)-2-methyl-3-phenylallyloxy]methane following the previously reported procedure [33]. The structure of the title compound was established on the basis of ^{1}H and ^{13}C NMR spectra, mass spectrum, microanalytical data [33], in addition to X-ray spectra [34]. In the title compound, $C_{20}H_{20}N_2O_3$, the ten atoms comprising the quinazoline ring are essentially planar and this plane is almost orthogonal to the terminal phenyl ring. The conformation about the ethylene bond is *E* and there is a significant twist between this residue and the adjacent phenyl ring. The crystal structure features centro-symmetric dimeric units linked by pairs of N—H...O hydrogen bonds between the amide groups which lead to eight membered $(\cdots HNCO)_2$ synthons. These are consolidated into a three dimensional architecture by C—H···O, C—H···π and π–π interactions. The FT-IR spectrum (Fig. 1) was recorded using KBr pellets on a DR/JASCO FT-IR 6300 spectrometer. The FT-Raman spectrum (Fig. 2) was obtained on a Bruker RFS 100/s, Germany. For excitation of the spectrum, the emission of Nd:YAG laser was used with an excitation wavelength of 1064 nm, a maximal power 150 mW; measurement on solid sample.

Computational details

Calculations of the title compound were carried out with Gaussian09 software [35] program using B3PW91/6-31G(d) (6D, 7F) and B3LYP/6-31G(d) (6D, 7F) basis sets to predict the molecular structure and vibrational wavenumbers. Calculations were carried out with Becke's three parameter hybrid model using the Lee–Yang–Parr correlation functional (B3LYP) method. Molecular geometries were fully optimized by Berny's optimization algorithm using redundant internal coordinates. Harmonic vibrational wavenumbers were calculated using analytic second derivatives to confirm the convergence to minima on the potential surface. Then frequency calculations were employed to confirm the structure as minimum points in energy. At the optimized structure (Fig. 3) of the examined species, no imaginary wavenumber modes were

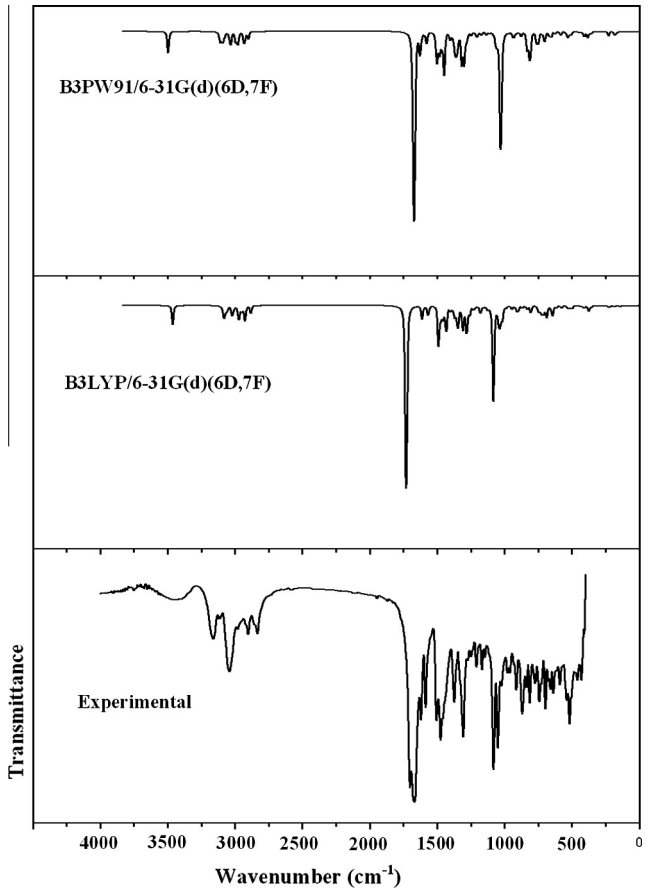

Fig. 1. FT-IR spectrum of 6-methyl-1-({[(2E)-2-methyl-3-phenyl-prop-2-en-1-yl]oxy}methyl)-1,2,3,4-tetra-hydroquinazoline-2,4-dione.

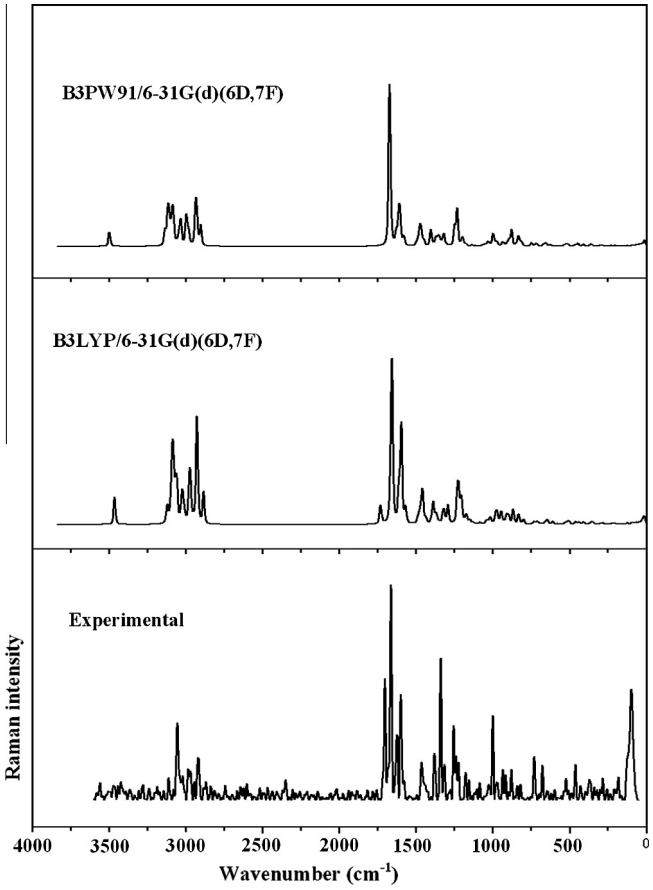

Fig. 2. FT-Raman spectrum of 6-methyl-1-({[(2E)-2-methyl-3-phenyl-prop-2-en-1-yl]oxy}methyl)-1,2,3,4-tetra-hydroquinazoline-2,4-dione.

obtained, proving that a true minimum on the potential surface was found. The DFT method tends to overestimate the fundamental modes; therefore scaling factor (0.9613) has to be used for obtaining a considerably better agreement with experimental data [36]. The observed disagreement between theory and experiment could be a consequence of the anharmonicity and of the general tendency of the quantum chemical methods to overestimate the force constants at the exact equilibrium geometry [36]. The optimized geometrical parameters (B3LYP/6-31G(d) (6D, 7F)) with XRD data are given in Table S1 (supporting material). The assignments of the calculated wavenumbers are aided by the animation option of GAUSSVIEW program, which gives a visual presentation of the vibrational modes [37]. The potential energy distribution (PED) is calculated with the help of GAR2PED software package [38].

Results and discussion

IR and Raman spectra

The calculated (scaled) wavenumbers, observed IR and Raman bands and assignments are given in Table 1. In the following discussion, the mono-substituted phenyl ring, tri-substituted phenyl ring and quinazoline rings are designated as PhI, PhII and Ring, respectively. The NH stretching vibrations give rise to bands at 3500–3300 cm^{-1} [39,40]. In the present study, the bands observed at 3448 cm^{-1} in the IR spectrum, 3467 cm^{-1} in the Raman spectrum and 3463 cm^{-1} (B3LYP) was assigned as NH stretching vibration. The N—H group shows bands at 1510–1500, 1350–1250 and 740–730 cm^{-1} [41]. According to the literature, if N—H is a part of a closed ring, the C—N—H deformation band is absent in the region 1510–1500 cm^{-1} [41,42]. For the title compound, the C—N—H deformation band is observed at 1369 cm^{-1} theoretically (B3LYP). The out of plane NH deformation is expected in the region 650 ± 50 cm^{-1} [42]. The band at 695 cm^{-1} experimentally and 690 cm^{-1} in B3LYP are assigned as this mode. Minitha et al. reported υNH at 3469 cm^{-1}, δNH at 1300 cm^{-1} [43]. Panicker et al. reported the out-of-plane bending mode of NH at 746 cm^{-1}, theoretically [44].

The CN stretching modes are expected in the range 1100–1300 cm^{-1} [45]. The bands observed at 1329, 1275, 1208 cm^{-1} in the IR spectrum, 1279, 1205, 1121 cm^{-1} in the Raman spectrum and at 1323, 1281, 1204, 1182, 1125, 1035 cm^{-1} theoretically (B3LYP) are assigned as CN stretching modes. Panicker et al. reported the CN stretching mode at 1215 cm^{-1} theoretically [44]

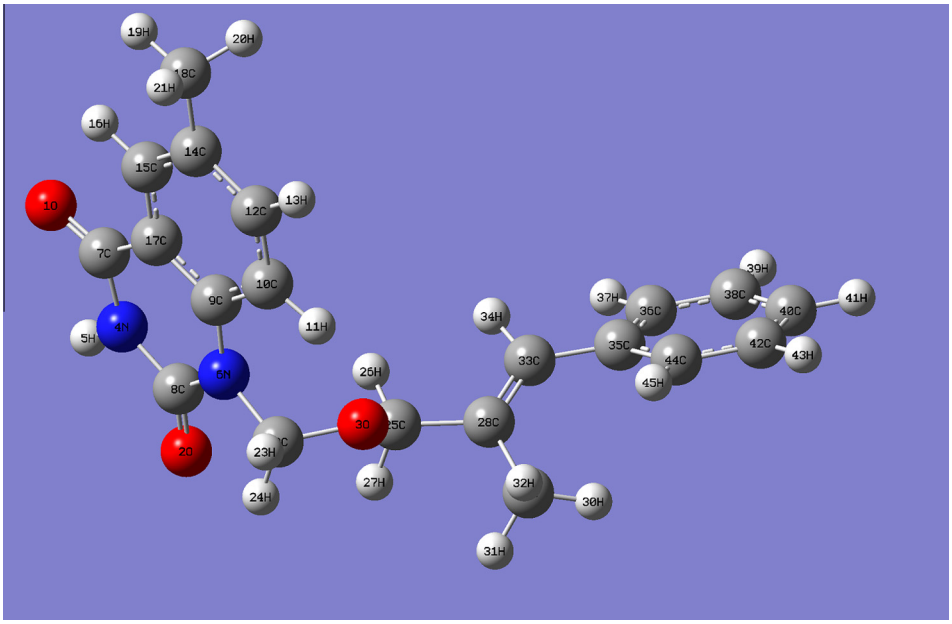

Fig. 3. Optimized geometry (B3LYP) of 6-methyl-1-({[(2E)-2-methyl-3-phenyl-prop-2-en-1-yl]oxy}methyl)-1,2,3,4-tetra-hydroquinazoline-2,4-dione.

Table 1
Vibrational assignments of the title compound.

B3PW91/6-31G(d) (6D, 7F)			B3LYP/6-31G(d) (6D, 7F)			IR	Raman	Assignments[a]
υ	IR_I	R_A	υ	IR_I	R_A	υ	υ	–
3497	78.86	110.28	3463	74.62	121.88	3448	3467	υNH(100)
3137	0.75	88.31	3121	1.16	86.42	3117	3115	υCHII(98)
3116	10.65	199.46	3095	8.76	116.19	–	–	υCHI(99)
3108	2.76	56.13	3090	2.71	62.66	–	3088	υCHII(99)
3107	37.39	124.37	3083	36.33	222.14	–	3080	υCHI(92)
3094	26.13	89.90	3072	28.57	91.94	–	–	υCHI(96)
3085	12.50	89.51	3062	0.39	113.83	–	–	υCHI(95)
3082	0.26	105.95	3061	13.84	95.67	–	–	υCHII(98)
3075	6.16	25.76	3055	6.58	26.55	–	3054	υCHI(98)
3053	5.03	47.87	3029	5.23	40.14	3035	–	$υ_{as}CH_2$(99)
3040	17.05	49.04	3023	16.62	53.32	–	–	$υ_{as}CH_3$(99)
3032	11.80	60.99	3020	20.15	53.94	–	3020	υCH(98)
3032	20.86	61.63	3011	13.38	61.15	–	3005	$υ_{as}CH_3$(99)
2999	17.26	111.43	2976	18.96	112.25	2977	2980	$υ_{as}CH_3$(99)
2994	18.70	80.00	2974	31.59	91.11	–	–	$υ_{as}CH_2$(99)
2984	17.67	89.01	2971	18.71	79.65	–	2966	$υ_{as}CH_3$(99)
2978	34.51	24.31	2950	31.93	23.20	–	2945	$υ_sCH_2$(99)
2933	33.37	263.42	2927	34.98	253.33	–	–	$υ_sCH_3$(100)
2932	26.63	176.82	2926	25.03	169.15	2925	2920	$υ_sCH_3$(100)
2904	25.29	120.10	2884	28.63	114.44	2868	2882	$υ_sCH_2$(99)
1676	666.76	20.06	1732	371.16	42.69	–	–	υC═O(75)
1673	0.30	644.90	1730	673.82	24.74	1720	1712	υC═O(69)
1667	272.70	55.87	1659	0.44	601.40	1665	1662	υC═C(65)
1627	92.81	70.65	1614	49.07	77.20	1617	1620	υPhII(67)
1609	3.74	269.59	1598	3.58	292.75	1588	1599	υPhI(61)
1581	40.47	26.10	1570	1.40	20.42	–	1575	υPhI(78)
1580	1.10	16.26	1567	43.88	24.08	–	–	υPhII(68)
1504	134.07	5.32	1491	142.80	4.49	1504	1496	υCNR(11), δCHII(12), υPhII(58)
1496	16.46	16.50	1486	12.20	19.00	–	–	δCHI(32), υPhI(61)
1484	26.99	6.91	1475	4.59	9.35	1476	–	$δCH_2$(83)
1483	29.76	15.96	1472	44.19	15.88	–	–	$δ_{as}CH_3$(68)
1473	7.99	48.73	1463	1.64	36.88	–	1464	$δ_{as}CH_3$(52) $δCH_2$(31)
1470	10.15	25.25	1459	22.70	24.57	–	–	$δ_{as}CH_3$(45) $δCH_2$(39)
1469	7.90	24.23	1458	15.29	22.50	–	–	$δ_{as}CH_3$(59) $δCH_2$(15)
1463	39.02	24.29	1457	6.14	23.19	1455	–	$δ_sCH_3$(100)
1449	88.54	10.70	1436	9.55	14.96	–	1438	υPhI(61), δCHI(36)
1448	40.81	7.73	1435	134.37	5.44	–	–	$δ_sCH_3$(33), υPhII(35)
1406	17.06	10.07	1404	15.17	6.30	–	1402	$δCH_2$(64)
1404	3.73	44.32	1392	8.59	12.72	–	–	$δ_sCH_3$(50), $δCH_2$(13)
1400	5.93	18.61	1389	1.62	47.15	–	–	$δ_sCH_3$(91)
1383	12.78	2.46	1373	38.52	20.28	1373	1376	$δCH_2$(64), $δCH_3$(13)
1382	8.63	4.04	1369	8.73	7.58	–	–	δNH(49), $δCH_2$(15), $δ_sCH_3$(16)
1370	41.64	26.97	1359	10.27	9.62	–	–	δCH(41), $δ_sCH_3$(19), $δCH_2$(15)
1359	68.02	18.58	1349	124.33	4.73	–	1338	υCNR(10), δCHII(14), υPhII(45)
1350	55.73	48.23	1323	17.95	52.42	1329	–	$δCH_2$(41), υCNR(42)
1340	0.26	5.50	1316	0.20	4.25	–	1316	δCHI(50), υPhI(41)
1323	10.49	39.61	1308	100.52	5.70	1309	–	υPhII(50), υPhI(21)
1318	92.02	22.61	1293	1.48	42.82	–	–	υPhI(62), δCHI(10)
1300	110.56	6.19	1281	148.04	4.67	1275	1279	υCNR(40), $δCH_2$(17), δCHII(15)
1281	36.40	1.81	1259	29.32	2.08	1248	1255	δCHII(45), υPhII(17)
1250	10.09	66.09	1233	10.18	58.16	–	1236	$δCH_2$(42), υCNR(20)
1233	3.03	137.73	1222	7.24	86.40	–	1223	δCH2(47), υCNR(18)
1209	14.03	1.64	1204	1.17	74.21	1208	1205	υCN(44), υPhI(27)
1204	6.21	9.41	1182	24.91	0.65	–	–	υCC(19), υCNR(42), δCHII(12)
1199	3.16	24.25	1176	5.33	22.25	–	1177	υCC(45), δCH(15)
1192	0.16	9.52	1170	0.16	8.70	1166	–	δCHI(73), υPhI(13)
1175	3.80	3.67	1157	6.77	5.02	–	1156	δCHII(51), υPhII(20)
1175	9.57	6.99	1147	0.01	8.59	1144	1142	δCHI(77), υPhI(14)
1135	11.54	5.94	1125	20.15	6.49	–	1121	$δCH_2$(27), υCNR(44), υCN(10)
1111	4.74	1.83	1100	6.11	1.09	1109	–	δCHII(41), υPhII(38)
1084	4.47	0.75	1083	440/83	5.51	1083	1085	υCO(66)
1065	40.63	5.74	1071	3.92	0.67	–	–	υPhI(37), δCHI(53)
1060	9.87	0.25	1045	77.70	9.45	1048	–	$δCH_3$(40), $δCH_2$(10), δPhII(38)
1053	25.41	6.56	1037	6.74	0.39	–	–	$δCH_3$(66)
1038	5.63	4.65	1035	52.29	4.46	–	–	δPhII(26), υCN(41)
1032	205.87	9.45	1024	22.94	5.10	–	1027	δCHI(16), $δCH_3$(42)
1026	232.39	8.43	1015	38.42	13.47	1019	–	δCHI(43), υPhI(25), $δCH_3$(17)
1009	7.87	5.17	992	8.09	5.28	–	–	$δCH_3$(71)
997	0.18	40.78	977	0.27	45.74	979	972	δPhI(17), υPhI(56)
995	1.04	9.23	968	0.50	9.28	964	–	$δCH_2$(49), $δCH_3$(18)
977	3.21	15.86	957	0.31	0.69	–	–	γCHI(80)
973	1.09	4.40	945	11.47	31.23	–	–	υCO(42), υCNR(10)
968	0.39	4.24	937	1.68	1.29	934	–	γCHII(89)

(*continued on next page*)

Table 1 (*continued*)

B3PW91/6-31G(d) (6D, 7F)			B3LYP/6-31G(d) (6D, 7F)			IR	Raman	Assignments[a]
υ	IR_I	R_A	υ	IR_I	R_A	υ	υ	–
939	13.81	10.12	932	0.46	2.81	–	934	γCHI(92)
929	1.88	1.99	914	14.54	17.40	914	915	υCC(34), υCNR(10), δCH_2(36)
928	9.72	6.15	902	12.62	9.73	–	–	γCHI(61)
910	3.85	5.60	901	3.48	3.33	–	–	γCHII(69), τPhII(10)
898	1.36	26.42	895	6.99	11.69	–	897	υCC(44), γCHII(13), δPhII(10)
879	15.68	63.04	867	9.76	36.25	870	863	γCH(35), υCC(32)
848	0.14	8.04	833	12.91	20.16	838	837	γCH(17), υCC(31), γCHI(16)
835	25.35	6.05	828	0.23	5.94	–	824	γCHI(97)
831	42.13	38.12	807	25.52	1.95	811	–	γCHII(82)
814	52.95	9.91	799	2.91	10.06	780	–	υCC(29), δCC(24)
812	89.16	8.70	751	12.54	0.10	–	753	γC═O(38), τPhII(22), τRing(27)
765	24.60	0.55	745	21.33	0.77	742	–	δRing(27), υCN(17), δCO(18)
756	19.41	1.21	733	19.57	7.43	–	730	τPhI(29), γCHI(48)
748	23.14	9.69	718	37.24	2.17	722	–	γC═O(47), γNH(17), τRing(17)
724	5.35	7.39	709	25.39	9.49	–	–	δPhII(24), γC═O(21), τRing(19)
714	3.78	5.43	690	28.84	0.33	695	695	τPhII(30), γNH(43), γC═O(10)
702	39.03	1.56	687	22.47	1.67	678	678	τPhI(60), γCHI(30)
670	7.34	4.33	658	5.26	7.01	660	–	δPhII(18), δPhI(25), δC═O(26)
664	9.07	5.16	648	25.49	6.45	–	–	γNH(19), τPhII(28), δPhI(27)
653	14.09	9.49	643	21.91	5.12	639	645	τPhII(22), γNH(21), γC═O(16)
626	6.69	2.32	617	6.64	2.16	–	619	δPhII(32), δRing(25)
624	0.54	4.96	609	0.27	4.79	612	598	δPhI(82)
585	11.23	2.27	578	10.74	1.87	584	–	δCO(24), δPhI(23), δPhII(15)
542	5.13	1.80	535	7.01	2.96	540	536	δPhI(17), τPhII(16), δCC(18)
530	16.89	4.36	523	8.76	2.75	519	524	τPhII(27), γCC(23), τRing(10)
518	6.21	6.74	510	3.67	7.01	–	–	τPhI(29), γCC(18), τCH_3(11)
509	13.02	6.42	501	15.62	5.60	503	505	δRing(26), τPhI(21), δCC(10)
466	1.01	6.41	462	0.71	5.70	459	462	γC═C(34), τPhI(12), δCC(12)
446	2.37	8.57	440	3.01	6.80	–	–	δC═O(22), δPhII(23), δRing(19)
433	2.76	0.89	425	1.07	0.39	428	428	τPhII(61), τRing(17)
412	6.80	2.89	412	8.79	3.14	–	–	δCN(23), δRing(21), δCH_2(20)
408	10.92	4.47	405	1.35	3.91	407	399	τPhI(77)
384	18.44	1.08	378	21.00	0.69	–	375	δC═O(22), δRing(29), τPhII(18)
364	7.67	4.37	362	7.59	4.65	–	–	δRing(22), δPhII(20), δCH_2(18)
360	1.43	3.16	352	0.59	1.50	–	–	δCC(30), δPhII(20)
354	1.17	1.66	349	1.58	2.19	–	–	δCC(22), τPhII(13), τCH_3(25)
349	0.32	1.44	344	0.08	1.46	–	341	τCC(31), τPhI(13), τCH_3(22)
303	1.68	3.01	301	1.62	2.56	–	301	δC═C(16), δCN(12), δPhI(10), γCC(11)
284	0.66	3.55	282	0.79	3.26	–	285	τPhI(35), δC═C(13), δCC(17)
230	2.64	1.32	229	6.15	0.95	–	232	δCC(26), δCN(16), δCH_2(15)
229	10.24	1.50	218	3.04	2.07	–	–	γCN(23), τRing(18), τCH_3(22)
204	0.12	2.94	204	0.38	1.99	–	207	τCH_3(35), γCN(14), δCC(12)
183	9.53	0.47	183	5.27	0.56	––	182	δCN(14), δCC(16), τCH_3(10), τCH_2(10)
179	5.44	0.27	168	0.64	0.12	–	–	τCH_3(17), δCO(12), τRing(12), δCC(10)
169	1.12	0.10	161	1.58	0.77	–	163	τRing(47), τNH(21)
157	1.46	0.87	143	3.32	0.36	–	–	τRing(53), τNH(40)
122	2.43	3.29	124	1.53	3.11	–	123	γCC(24), τCH_2(13), τPhI(11)
95	0.85	3.23	96	0.69	3.15	–	97	τCH_3(24), τC═C(12), τRing(11)
82	0.51	1.85	81	0.37	2.27	–	–	γCN(16), τC═C(14), τPhII(11), τRing(17)
65	0.49	4.25	66	0.40	3.66	–	–	τC═C(16), τRing(39), τPhII(15)
47	1.02	3.41	49	0.71	3.12	–	–	τC═C(28), τCH_3(13), τCN(12), τCC(23)
43	0.04	3.52	43	0.01	2.26	–	–	τC═C(25), τRing(19), τCN(16)
27	0.45	6.73	36	0.06	0.32	–	–	τCH_3(67), γCC(17)
19	0.20	1.35	27	0.47	7.45	–	–	τC═C(37), τCC(14), τCN(14)
14	0.97	9.00	17	0.66	9.49	–	–	τCO(54), τCN(18), τCH_2(20)
11	0.05	7.85	12	0.04	8.41	–	–	τCO(41), τCN(16), τCH_2(17)

[a] υ – stretching; δ – in-plane deformation; γ – out-of-plane deformation; τ – torsion; as – asymmetric; s – symmetric; PhI – mono-substituted phenyl ring; PhII – tri substituted phenyl ring; Ring – quinazoline; IR_I – IR intensity; R_A – Raman activity. Potential energy distribution is given in brackets in the assignment column.

and Ulahannan et al. [46,47] reported CN stretching modes at 1262 cm^{-1} in IR, 1244, 1202 cm^{-1} in the Raman spectrum and at 1270, 1255, 1240, 1230 cm^{-1} theoretically.

The carbonyl group is contained in a large number of different classes of compounds, for which a strong absorption band due to C═O stretching vibration is observed in the range of 1850–1550 cm^{-1} [41]. The carbonyl groups give rise to bands at 1720–1790 cm^{-1} [48]. For the title compound, the C═O stretching bands are observed at 1720 cm^{-1} in the IR spectrum, 1712 cm^{-1} in the Raman spectrum and at 1732, 1730 cm^{-1} theoretically. The deformation modes of the C═O group are also identified and assigned (Table 1). For the title compound, as expected the asymmetric C—O—C stretching vibration is assigned at 1083 cm^{-1} and the symmetric stretching mode at 945 cm^{-1} theoretically (B3LYP) [49]. Experimentally, these modes are observed at 1083 cm^{-1} in the IR spectrum and at 1085 cm^{-1} in the Raman spectrum for the title compound. Bhagyasree et al. [50] reported C—O—C stretching modes at 1144, 1063 (IR), 1146, 1066 (Raman) and at 1153, 1079 cm^{-1} theoretically (SDD). The skeleton C—O deformations can be found in the region 320 ± 50 cm^{-1} [51].

The vibrations of the CH_2 group, the asymmetric stretch $\upsilon_{as}CH_2$, symmetric stretch $\upsilon_s CH_2$, scissoring vibration δCH_2, appear in the

region 2945 ± 45, 2885 ± 45 and 1445 ± 35 cm^{-1}, respectively [42,52]. The B3LYP calculations give $\upsilon_{as}CH_2$ at 3029, 2974 cm^{-1} and υ_sCH_2 at 2950, 2884 cm^{-1}. The bands observed at 3035, 2868 cm^{-1} (IR) and 2945, 2882 cm^{-1} (Raman) are assigned CH_2 modes stretching modes. In the present case, the band observed at 1476 cm^{-1} in the IR, 1402 cm^{-1} in Raman spectrum and 1475, 1404 cm^{-1} (B3LYP) are assigned as the scissoring mode of CH_2. Bands of hydrocarbons due to CH_2 twisting and wagging vibrations are observed in the region 1180–1390 cm^{-1} [49,52]. The CH_2 wagging and twisting modes are assigned at 1373, 1323, 1233, 1222 cm^{-1} (B3LYP), 1373, 1329 cm^{-1} (IR), 1376, 1236, 1223 cm^{-1} (Raman), respectively. The bands calculated at 968, 914 cm^{-1} are assigned as the rocking modes of CH_2.

The stretching vibrations of the CH_3 group are expected in the range of 2900–3050 cm^{-1} [42,52]. The asymmetric stretching modes of the methyl group are calculated to be at 3023, 3011, 2976, 2971 cm^{-1} and the symmetric modes at 2927, 2926 cm^{-1}. The bands observed at 2977, 2925 cm^{-1} in the infrared spectrum and at 3005, 2980, 2966, 2920 cm^{-1} in the Raman spectrum were assigned as stretching modes of the CH_3 group. The asymmetric and symmetric bending vibrations of the methyl group normally appear in the region of 1400–1485 cm^{-1} and 1380–1420 cm^{-1} [41,42]. The bands observed at 1455 cm^{-1} in the IR spectrum and at 1464 cm^{-1} in the Raman spectrum were assigned as CH_3 bending modes. The B3LYP calculations give these modes in the range 1389–1472 cm^{-1}. In the present case the rocking modes of methyl group were calculated to be at 1045, 1037, 1024, 992 cm^{-1} and were observed at 1048 cm^{-1} in the IR spectrum and at 1027 cm^{-1} in the Raman spectrum. The torsional vibrations of methyl groups were often assigned within the region 185 ± 65 cm^{-1} [42]. The CC modes are also identified and assigned (Table 1).

The existence of one or more aromatic rings in the structure is normally readily determined from the C—H and C=C—C ring related vibrations. The C—H stretching occurs above 3000 cm^{-1} and is typically exhibited as a multiplicity of weak to moderate bands, compared with the aliphatic C—H stretch [53]. The bands observed at 3117 cm^{-1} in the IR and 3115, 3088, 3080, 3054 cm^{-1} in the Raman spectrum are assigned as the C—H stretching modes of the phenyl rings. The B3LYP calculations give these modes in the range 3055–3121 cm^{-1}.

The benzene ring possesses six ring stretching vibrations, of which the four with the highest wavenumbers (occurring near 1600, 1580, 1490 and 1440 cm^{-1}) are good group vibrations. In the absence of ring conjugation, the band near 1580 cm^{-1} is usually weaker than that at 1600 cm^{-1}. The fifth ring stretching vibration which is active near 1335 ± 35 cm^{-1} a region which overlaps strongly with that of the CH in-plane deformation and the intensity is in general is low or medium high [42]. The sixth ring stretching vibration or ring breathing mode appears as a weak band near 1000 cm^{-1} in mono, 1,3-di and 1,3,5-trisubstituted benzenes. However, in the otherwise substituted benzene, this vibration is substituent sensitive and difficult to distinguish from the ring in-plane deformation. Since the identification of all the normal modes of vibrations of large molecules is not trivial, we tried to simplify the problem by considering each molecule as substituted benzene. Such an idea has already been successfully utilized by several workers for the vibrational assignments of molecules containing multiple homo- and hetero-aromatic rings [50,54–56]. The modes in the two phenyl rings will differ in wavenumber and the magnitude of splitting will depend on the strength of interactions between different parts (internal coordinates) of the two rings. For some modes, this splitting is so small that they may be considered as quasi-degenerate and for the other modes a significant amount of splitting is observed. Such observations have already been reported [50,54–56].

For the title compound, the bands observed at 1617, 1504, 1309 cm^{-1} in the IR and 1620, 1496, 1338 cm^{-1} in the Raman spectrum are assigned as υPhII modes with 1614, 1567, 1491, 1349, 1308 cm^{-1} as B3LYP values. In asymmetric tri-substituted benzene, when all the three substituents are light, the ring breathing mode falls in the range 500–600 cm^{-1}; when all the three substituents are heavy, it appears in the range 1050–1100 cm^{-1} and in the case of mixed substituents, it falls in the range 600–750 cm^{-1} [57]. Madhavan et al. [58] reported the ring breathing mode for a compound having two tri-substituted benzene rings as 1110 cm^{-1} and 1129 cm^{-1}. For the title compound, PED analysis gives the ring breathing mode at 1100 cm^{-1} (B3LYP) with 1109 cm^{-1} in IR which is in agreement with the literature [50,59]. For tri-substituted benzenes δCH modes are expected in the range 1100–1280 cm^{-1} [42]. For the phenyl ring PhII, the bands observed at 1248, 1109 cm^{-1} in the IR spectrum and at 1255, 1156 cm^{-1} in the Raman spectrum are assigned as in-plane CH deformation modes. Also B3LYP calculations give these modes at 1259, 1157, 1100 cm^{-1} which are in agreement with the literature [42].

For mono-substituted benzene, the υPh modes are expected in the range of 1285–1610 cm^{-1} [42]. For the title compound, the υPhI modes are assigned at 1598, 1570, 1486, 1436, 1293 cm^{-1} theoretically and bands are observed at 1588 cm^{-1} in IR spectrum and at 1599, 1575, 1438 cm^{-1} in Raman spectrum. The ring breathing mode for mono-substituted benzenes appears near 1000 cm^{-1} [42]. For the title compound, this is confirmed by the band at 979 cm^{-1} in the IR spectrum which finds support from the computational results 977 cm^{-1}. For mono-substituted benzene, the in-plane CH vibrations are expected in the range of 1015–1300 cm^{-1} [42]. Bands observed at 1166, 1144, 1019 cm^{-1} in the IR spectrum and at 1316, 1142 cm^{-1} in the Raman spectrum are assigned as δCH modes for the ring PhI. The corresponding theoretical values (B3LYP) are 1316, 1170, 1147, 1071 and 1015 cm^{-1}.

The C—H out-of-plane deformations γCH are observed between 1000 and 700 cm^{-1} [42]. γCH vibrations are mainly determined by the number of adjacent hydrogen atoms on the ring. Although strongly electron attracting substituent groups, such as nitro group can result in an increase (about 30 cm^{-1}) in the wavenumber of the vibration, these vibrations are not very much affected by the nature of the substituent. Generally the C—H out-of-plane deformations with the highest wavenumbers have a weaker intensity than those absorbing at lower wavenumbers. Most of the deformation bands of the CH vibrations of the phenyl rings are not pure but contain significant contributions for other modes (Table 1). The out-of-plane γCH modes are observed at 934, 811 cm^{-1} in the IR spectrum, for PhII and at 934, 824, 730 cm^{-1} in Raman spectrum for PhI. The corresponding B3LYP values are 937, 901, 807 cm^{-1} for PhII and 957, 932, 902, 828, 733 cm^{-1} for PhI.

In order to investigate the performance of vibrational wavenumbers of the title compound, the root mean square (RMS) value between the calculated and observed wavenumbers were calculated. The RMS values of wavenumbers were calculated using the following expression [51]:

$$\mathrm{RMS} = \sqrt{\frac{1}{n-1}\sum_i^n \left(\upsilon_i^{calc} - \upsilon_i^{exp}\right)^2}$$

The RMS errors of the observed IR and Raman bands are found to be 19.93 and 17.79 for B3PW91/6-31G(d) (6D, 7F) and 7.14 and 4.50 for B3LYP/6-31G(d) (6D, 7F) methods, respectively. The small differences between experimental and calculated vibrational modes are observed. This is due to the fact that experimental results belong to solid phase and theoretical calculations belong to gaseous phase.

NLO properties

Nonlinear optical (NLO) effects arise from the interactions of electromagnetic fields in various media to produce new fields altered in phase, frequency, amplitude or other propagation characteristic from the incident fields. The first order hyperpolarizabilty (β) of the title molecule is calculated using B3LYP method. The first order hyperpolarizability is a third rank tensor that can be described by $3 \times 3 \times 3$ matrices. The 27 components of the 3D matrix can be reduced to 10 components due to the Kleinman symmetry [60]. It can be given in the lower tetrahedral format. It is obvious that the lower part of the $3 \times 3 \times 3$ matrices is a tetrahedral. The components of β are defined as the coefficients in the Taylor series expansion of the energy in the external electric field. When the external electric field is weak and homogenous, this expansion becomes:

$$E = E_0 - \sum_i \mu_i F^i - \frac{1}{2}\sum_{ij} \alpha_{ij} F^i F^j - \frac{1}{6}\sum_{ijk} \beta_{ijk} F^i F^j F^k - \frac{1}{24}\sum_{ijkl} \gamma_{ijkl} F^i F^j F^k F^l + \cdots$$

where E_0 is the energy of the unperturbed molecule, F^i is the field at the origin, μ_{ij}, α_{ij}, β_{ijk} and γ_{ijkl} are the components of dipole moment, polarizability, the first hyperpolarizabilities, and second hyperpolarizibilities, respectively. The calculated first hyper polarizability of the title compound is 2.75×10^{-30} esu and which is 21.15 times that of the standard NLO material urea (0.13×10^{-30} esu) [61]. We conclude that the title compound is an attractive object for future studies of nonlinear optical properties.

Frontier molecular orbital analysis

The most widely used theory by chemists is the molecular orbital (MO) theory. It is important that ionization potential I, electron affinity A, electrophilicity index ω, chemical potential μ, electronegativity χ, hardness η and softness χ be put into a MO framework. Based on density functional descriptors and global chemical reactivity descriptors of compounds such as hardness, chemical potential, softness, electronegativity and electrophilicity index as well as local reactivity has been defined [62–64]. Pauling introduced the concept of electronegativity as the power of an atom in a compound to attract electrons to it. Using Koopman's theorem for closed shell components η, μ and χ can be defined as $\eta = I - A$; $\mu = (I - A)/2$; $\chi = (I + A)/2$; where I and A are the ionization potential and electron affinity of the compounds respectively. The ionization energy and electron affinity can be expressed through HOMO and LUMO orbital energies as $I = -E_{HOMO}$ (6.456) and $A = -E_{LUMO}$ (0.140). Electron affinity refers to the capability of ligand to accept precisely one electron from a donor. However, in many kinds of bonding viz. covalent and hydrogen bonding, partial charge transfer takes place. The ionization potential given by DFT method for the title compound is 6.456 eV. Considering the chemical hardness, large HOMO–LUMO gap means a hard molecule and small HOMO–LUMO gap means a soft molecule. One can also relate the stability of the molecule to hardness, which means that the molecule with least HOMO–LUMO gap means, it is more reactive. Parr et al. [62] have defined a new descriptor to quantity the global electrophilic power of the compound as electrophilicity index (ω) which defines a quantitative classification of global electrophilic nature of a compound. Parr et al. have proposed electrophilicity index (ω) as a measure of energy lowering due to maximal electron flow between donor and acceptor. They defined electrophilicity index as follows: $\omega = \mu^2/2\eta$. The usefulness of this new reactivity quantity has been recently demonstrated understanding the toxicity of various pollutants in terms of their reactivity and site selectivity [65]. The calculated vales of hardness, softness and electrophilicity index are 6.316, 3.298 and 0.7895. When two molecules react, which one will act as an electrophile (nucleophile) will depend on which one has a higher (lower) electrophilicity index [66]. The calculated value of electrophilicity index describes the biological activity of the title compound. The atomic orbital components of the frontier molecular orbital are shown in Fig. 4.

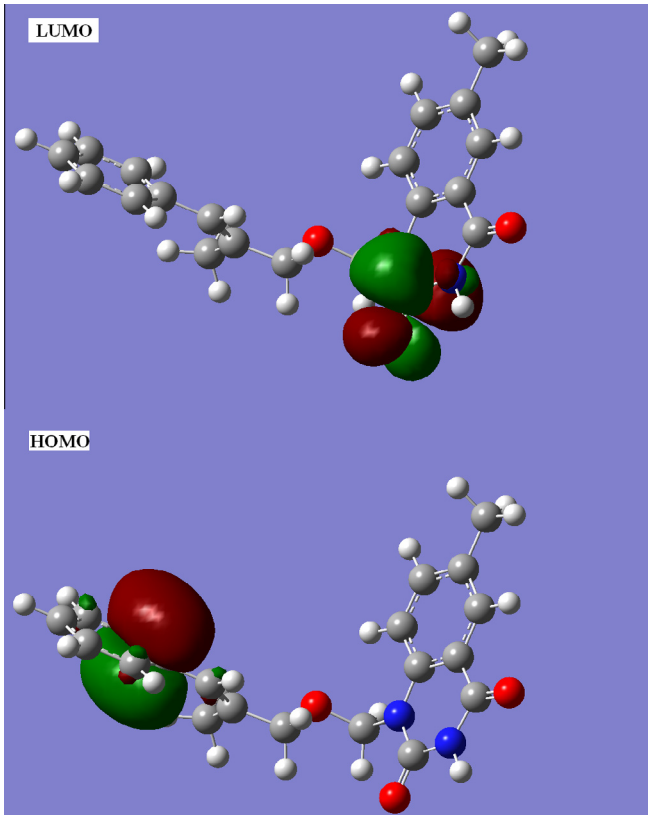

Fig. 4. HOMO and LUMO plots of the title compound.

Molecular electrostatic potential

MEP is related to the ED and is a very useful descriptor in understanding sites for electrophilic and nucleophilic reactions as well as hydrogen bonding interactions [67,68]. The electrostatic potential $V(r)$ is also well suited for analyzing processes based on the "recognition" of one molecule by another, as in drug–receptor, and enzyme–substrate interactions, because it is through their potentials that the two species first "see" each other [69,70]. To predict reactive sites of electrophilic and nucleophilic attacks for the investigated molecule, MEP at the B3LYP/6-31G(d,p) optimized geometry was calculated. The negative (red and yellow) regions of MEP were related to electrophilic reactivity and the positive (blue[1]) regions to nucleophilic reactivity (Fig. 5). From the MEP it is evident that the negative charge covers the C=O group and the positive region is over the phenyl ring and NH group.

NBO analysis

The natural bonding orbital (NBO) analysis has been performed in order to investigate intra-molecular charge transfer interactions,

[1] For interpretation of color in Fig. 5, the reader is referred to the web version of this article.

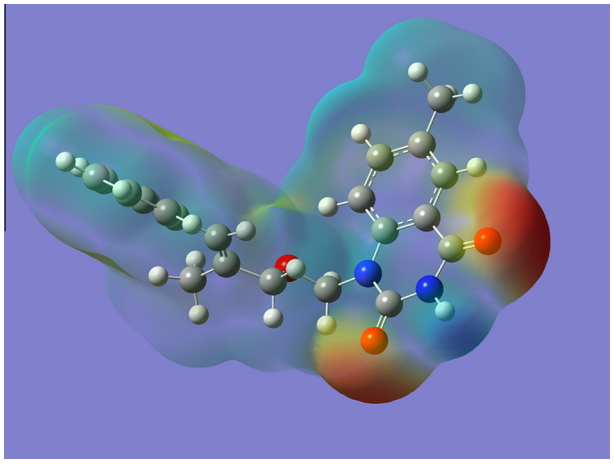

Fig. 5. MEP plot of the title compound.

re-hybridization and delocalization of electron density within the molecule. The hyper-conjugation may be given as stabilizing effect that arises from an overlap between an occupied orbital with another neighboring electron deficient orbital, when these orbitals are properly oriented. This non-covalent bonding (anti-bonding) interaction can be quantitatively described in terms of the NBO analysis, which is expressed by means of the second order perturbation interaction energy $E(2)$ [71–74]. This energy represents the estimate of the off diagonal NBO Fock matrix elements. It can be deduced from the second order perturbation approach [75] and is given as:

$$E(2) = \Delta E_{ij} = q_i \frac{(F_{i,j})^2}{(E_j - E_i)}$$

where q_i is the donor orbital occupancy, E_i and E_j are the diagonal elements and $F_{i,j}$ is the off diagonal NBO Fock matrix element.

The intra-molecular hyper-conjugative interactions are formed by the orbital overlap between n(O) and σ^*(C—N) bond orbital which results in ICT causing stabilization of the system. The strong intra-molecular hyper-conjugative interaction of N_4—C_7 from $n_2(O_1) \rightarrow \sigma^*(N_4—C_7)$ which increases ED (0.08610e) that weakens the respective bonds leading to stabilization of 28.56 kcal mol^{-1}. The strong intra-molecular hyper-conjugative interaction of N_6—C_8 from $n_2(O_2) \rightarrow \sigma^*(N_6—C_8)$ which increases ED (0.08893e) that weakens the respective bonds leading to stabilization of 26.99 kcal mol^{-1}. The strong intra-molecular hyper-conjugative interaction of N_4—C_9 from $n_2(O_3) \rightarrow \sigma^*(N_6—C_{22})$ which increases ED (0.05647e) that weakens the respective bonds leading to stabilization of 13.91 kcal mol^{-1}. Another intra-molecular hyper-conjugative interactions are also formed by the orbital overlap between n(N) and σ^*(O—C) bond orbital which results in ICT causing stabilization of the system. The strong intra-molecular hyper-conjugative interaction of O_2—C_8 from $n_1(N_4) \rightarrow \pi^*(O_2—C_8)$, $n_1(N_6) \rightarrow \pi^*(O_2—C_8)$ which increases ED (0.36925e) that weakens the respective bonds leading to stabilization of 60.15, 60.77 kcal mol^{-1}. The increased electron density at the different atoms leads to the elongation of respective bond length and a lowering of the corresponding stretching wavenumber. The electron density (ED) is transferred from the n(O) and n(N) to the anti-bonding π^*, σ^* orbitals of the C—N, C—O explaining both the elongation and the red shift. The C=O, N—C, and C—O—C stretching modes can be used as a good probe for evaluating bonding configuration around the corresponding atoms and the electronic distribution of the molecule.

The NBO analysis also describes the bonding in terms of the natural hybrid orbital $n_2(O_1)$, which occupy a higher energy orbital (−0.25003 a.u.) with considerable p-character (99.99%) and low occupation number (1.85914 a.u.) and the other $n_1(O_1)$ occupy a lower energy orbital (−0.67961 a.u.) with p-character (41.21%) and high occupation number (1.97719 a.u.). Also $n_2(O_2)$, which occupy a higher energy orbital (−0.25415 a.u.) with considerable p-character (100.00%) and low occupation number (1.84247 a.u.) and the other $n_1(O_2)$ occupy a lower energy orbital (−0.68772 a.u.) with p-character (40.24%) and high occupation number (1.97521 a.u.). Again $n_2(O_3)$, which occupy a higher energy orbital (−0.30357 a.u.) with considerable p-character (99.38%) and low occupation number (1.90846 a.u.) and the other $n_1(O_3)$ occupy a lower energy orbital (−0.56616 a.u.) with p-character (57.27%) and high occupation number (1.96527 a.u.). Thus, a very close to pure p-type lone pair orbital participates in the electron donation to the σ^*(C—N) orbital for $n_2(O_1) \rightarrow \sigma^*(N_4—C_7)$, σ^*(N—C) orbital for $n_2(O_2) \rightarrow \sigma^*(N_6—C_8)$, σ^*(N—C) orbital for $n_2(O_3) \rightarrow \sigma^*(N_6—C_{22})$ and π^*(O—C) orbital for $n_1(N_4) \rightarrow \pi^*(O_2—C_8)$, $n_1(N_6) \rightarrow \pi^*(O_2—C_8)$ interactions in the compound. The results are tabulated in Tables S2 and S3 (supporting material).

Geometrical parameters

The CC bond lengths in the ring PhI lie between 1.3925–1.4742 Å (B3LYP) and 1.3790–1.4790 Å (XRD) and in the ring PhII lies between 1.3891–1.4075 Å (B3LYP) and 1.3790–1.4000 Å (XRD). In the title compound, benzene rings are a regular hexagon with bond lengths somewhere in between the normal values for a single (1.54) and a double (1.33) bond [76]. For the title compound, the C=O bond lengths are 1.2207, 1.2216 Å (B3LYP), 1.2257, 1.2311 Å (XRD) and C—O bond lengths are 1.4010, 1.4385 Å (B3LYP), 1.4130, 1.4409 Å (XRD) which are in agreements with reported values [77–79]. In the title quinazoline ring, the bond lengths for the C_9—N_6, C_8—N_6, C_8—N_4, C_7—N_4 are 1.4070, 1.3945, 1.3885, 1.3945 Å (B3LYP) and 1.4081, 1.3749, 1.3773, 1.3780 Å (XRD), respectively. These bond lengths are indicative of a significant double bond character. The C—N bond lengths were also found to be much shorter than the average value for a C—N bond (1.47 Å), but significantly longer than a C=N double bond (1.22 Å) [80], suggesting that some multiple bond character is presented. At C_9 position of the Ring II, the bond angles C_{10}—C_9—N_6 = 121.5 and C_{17}—C_9—C_{10} = 118.4° and this asymmetry shows the interaction between Ring II and quinazoline ring. Also at C_6 and C_8 positions of the quinazoline ring, the bond angles given by B3LYP calculations are, C_9—N_6—C_8 = 122.4, C_8—N_6—C_{22} = 117.1, N_4—C_8—N_6 = 115.0, N_6—C_8—O_2 = 123.6°, which shows the interaction between O_2 and the CH_2 group at C_{22} position. The asymmetry of the bond angles at C_{35} position (C_{36}—C_{35}—C_{44} = 117.9, C_{36}—C_{35}—C_{33} = 118.6, C_{44}—C_{35}—C_{33} = 123.6°) gives the steric repulsion between Ring I and the adjacent groups.

The C=C group is tilted from the phenyl Ring I as is evident from the torsion angles, C_{38}—C_{36}—C_{35}—C_{33} = 179.7, C_{36}—C_{35}—C_{33}—C_{28} = −36.6, C_{42}—C_{44}—C_{35}—C_{33} = −179.3 and C_{44}—C_{35}—C_{33}—C_{38} = 145.7°. The torsion angles, C_{17}—C_9—N_6—C_{22} = −171.7, C_9—N_6—C_{22}—O_3 = −70.8, N_4—C_8—N_6—C_{22} = 173.6, C_8—N_6—C_{22}—O_3 = 112.1° show that the quinazoline ring and C_{22}—O_3 groups are tilted from each other. Most of the theoretically obtained geometrical parameters (B3LYP) are in agreement with the XRD data.

Conclusion

6-Methyl-1-({[(2E)-2-methyl-3-phenyl-prop-2-en-1-yl]oxy}-methyl)-1,2,3,4-tetra-hydro quinazoline-2,4-dione was prepared *via* treatment of silylated 6-methylquinazoline-2,4-dione with

bis-[(*E*)-2-methyl-3-phenylallyloxy]methane. The vibrational wavenumbers were examined theoretically using the Gaussian09 set of quantum chemistry codes, and the normal modes were assigned by potential energy distribution calculation. The geometrical parameters of the title compound are in agreement with the XRD results. A computation of the first hyperpolarizability indicates that the compound may be a good candidate as a NLO material. Stability of the molecule arising from hyper-conjugative interaction and charge delocalization has been analyzed using NBO analysis. The difference in HOMO and LUMO energy supports the charge transfer interaction within the molecule. To predict the reactive sites for electrophilic and nucleophilic attack for the title compound, the MEP at B3LYP optimized geometry was calculated.

Acknowledgements

The authors would like to extend their sincere appreciation to the Deanship of Scientific Research at King Saud University for funding this work through the Research Group Project No. RGP-VPP-274. CYP is thankful to University of Antwerp for access to the University's CalcUA supercomputer cluster and Dr. Hema Tresa Varghese, Department of Physics, FMN College, Kollam, Kerala, India, for providing computational facility.

Appendix A. Supplementary material

Supplementary data associated with this article can be found, in the online version, at http://dx.doi.org/10.1016/j.saa.2014.06.039.

References

[1] E.L. Ellsworth, T.P. Tran, H.D. Hollis Showalter, J.P. Sanchez, B.M. Watson, M.A. Stier, J.M. Domagala, S.J. Gracheck, E.T. Joannides, M.A. Shapiro, S.A. Dunham, D.L. Hanna, M.D. Huband, J.W. Gage, J.C. Bronstein, J.Y. Liu, D.Q. Nguyen, R. Singh, J. Med. Chem. 49 (2006) 6435–6438.
[2] V. Colotta, O. Lenzi, D. Catarzi, F. Varano, L. Squarcialupi, C. Costagli, A. Galli, C. Ghelardini, A.M. Pugliese, G. Maraula, E. Coppi, D.E. Pellegrini-Giampietro, F. Pedata, D. Sabbadin, S. Moro, Eur. J. Med. Chem. 54 (2012) 470–482.
[3] M. Zia-Ur-Rehman, J.A. Choudary, S. Ahmad, H.L. Siddiqui, Chem. Pharm. Bull. 54 (2006) 1175–1178.
[4] V. Alagarsamy, U.S. Pathak, D. Sriram, S.N. Pandeya, E. DeClercq, Indian J. Pharm. Sci. 62 (2000) 433–437.
[5] D. Carrico, M.A. Blaskovich, C.J. Bucher, S.M. Sebti, A.D. Hamilton, Bioorg. Med. Chem. 13 (2005) 677–688.
[6] D.W. Fry, A.J. Kraker, A. McMichael, L.A. Ambroso, J.M. Nelson, W.R. Leopold, R.W. Connors, A.J. Bridges, Science 265 (1994) 1093–1095.
[7] J. Dowell, J.D. Minna, P. Kirkpatrick, Nat. Rev. Drug Discov. 4 (2005) 13–14.
[8] M. Bos, J. Mondelsohn, Y.M. Kim, J. Albanell, D.W. Fry, J. Baselga, Clin. Cancer Res. 3 (1997) 2099–2106.
[9] T.M. Traxler, P. Furet, H. Mett, E. Buchdunger, T. Meyer, N. Lydon, J. Med. Chem. 39 (1996) 2285–2292.
[10] J.W. Corbett, S.S. Ko, J.D. Rodgers, S. Jeffrey, L.T. Bacheler, R.M. Klabe, S. Diamond, C.M. Lai, S.R. Rabel, J.A. Saye, S.P. Adams, C.L. Trainor, P.S. Anderson, S.K. Erichson-Vitanen, Antimicrob. Agents Chemother. 43 (1999) 2893–2897.
[11] R.O. Dempcy, E.B. Skibo, Biochemistry 30 (1991) 8480.
[12] V.K. Pandey, D. Mishra, S. Shukla, Indian Drugs 31 (1994) 532–536.
[13] M. Koller, K. Lingenhoehl, M. Schmutz, I.T. Vranesic, J. Kallen, Y.P. Auberson, D.A. Carcache, H. Mattes, S. Ofner, D. Orain, S. Urwyler, Med. Chem. Lett. 21 (2011) 3358–3361.
[14] M.K. Prashanth, M. Madaiah, H.D. Revanasiddappa, B. Veeresh, Spectrochim. Acta A 110 (2013) 324–332.
[15] H. Manabu, I. Ryvichi, H. Hideak, Chem. Pharm. Bull. 38 (1990) 618–622.
[16] V. Jatav, P. Mishra, S. Kashaw, J.P. Stables, Eur. J. Med. Chem. 43 (2008) 135–141.
[17] A.R. Maarouf, E.R. El-Bendary, F.E. Goda, Arch. Pharm. 337 (2004) 527–532.
[18] V. Alagarsamy, R. Giridhar, H.R. Yadav, R. Revathi, K. Rukmani, E. De Clercq, Indian J. Pharm. Sci. 68 (2006) 532.
[19] S.V. Bhandari, B.J. Deshmane, S.C. Dangare, S.T. Gore, V.T. Raparti, C.V. Khachane, A.P. Sarkate, Pharmacologyonline 2 (2008) 604.
[20] A.A. Bekhit, N.S. Habbib, A. Bekhit, Boll. Chim. Farm. 140 (2001) 297.
[21] M.R. Azza, E.R. Eman, G.E. Fatma, Arch. Pharm. 337 (2004) 527.
[22] V.K. Pandey, S. Tusi, Z. Tusi, R. Raghubir, M. Dixit, M.N. Joshi, Indian J. Chem. 43 (2004) 180.
[23] A. Kamal, V. Devaiah, N. Sankarajah, K.L. Reddy, Synlett 16 (2006) 2609.
[24] V. Alagarsamy, V.R. Saloman, G. Vanikavith, V. Paluchamy, M.R. Chandran, A.A. Sujin, A. Thangathiruppathy, S.A. Muthulakashmi, R. Revathi, Biol. Pharm. Bull. 25 (2002) 1432.
[25] M. Costa, N.D. Ca, B. Gabriele, C. Massera, G. Salerno, M. Soliani, J. Org. Chem. 69 (2004) 2469.
[26] G.R. Madhavan, R. Chakrabarti, S.K.B. Kumar, P. Misra, R.N.V.S. Mamidi, K. Balraju, R.K. Babu, J. Suresh, B.B. Loharyb, J. Iqbal, R. Rajagopalan, Eur. J. Med. Chem. 36 (2001) 627.
[27] C. Parkanyi, D.S. Schmidt, J. Heterocycl. Chem. 37 (2000) 725.
[28] P. Owalski, M.J. Mokrosz, Z. Majka, Y. Kowalska, J. Heterocycl. Chem. 37 (2000) 187.
[29] A. Wissner, D.M. Berger, D.H. Boschelli, B.C. Gruver, B.D. Johnson, N. Mamuya, Y.F. Wang, B.Q. Wu, F. Ye, N. Zhang, J. Med. Chem. 43 (2000) 3244.
[30] G.S. Chen, S. Kalchar, C.W. Kuo, C.S. Chang, C.O. Usifoh, J.W. Chern, J. Org. Chem. 68 (2003) 2502.
[31] A.K. Nanda, S. Ganguli, R. Chakraborty, Molecules 12 (2007) 2413.
[32] T. Hou, L. Zhu, L. Chen, X. Xu, J. Chem. Inf. Comput. Sci. 43 (2003) 273.
[33] N.R. El-Brollosy, J. Chem. Res. (2007) 358–361.
[34] N.R. El-Brollosy, M.I. Attia, A.A. El-Emam, S.W. Ng, E.R.T. Tiekink, Acta Crystallogr. E68 (2012) o1768–o1769.
[35] M.J. Frisch, G.W. Trucks, H.B. Schlegel, G.E. Scuseria, M.A. Robb, J.R. Cheeseman, G. Scalmani, V. Barone, B. Mennucci, G.A. Petersson, H. Nakatsuji, M. Caricato, X. Li, H.P. Hratchian, A.F. Izmaylov, J. Bloino, G. Zheng, J.L. Sonneberg, M. Hada, M. Ehara, K. Toyota, R. Fukuda, J. Hasegawa, M. Ishida, T. Nakajima, Y. Honda, O. Kitao, H. Nakai, T. Vreven, J.A. Montgomery, J.E. Peralta, F. Ogliaro, M. Bearpark, J.J. Heyd, E. Brothers, K.N. Kudin, V.N. Staroverov, T. Keith, R. Kobayashi, J. Normand, K. Raghavachari, A. Rendell, J.C. Knox, J.B. Cross, V. Bakken, C. Adamo, J. Jaramillo, R. Gomperts, R.E. Stratmann, O. Yazyev, A.J. Austin, R. Cammi, C. Pomelli, J.W. Ochterski, R.L. Martin, K. Morokuma, V.G. Zakrzewski, G.A. Voth, P. Salvador, J.J. Dannenberg, S. Dapprich, A.D. Daniels, O. Farkas, J.B. Foresman, J.V. Ortiz, J. Cioslowski, D.J. Fox, Gaussian09, Revision B.01, Gaussian Inc., Wallingford, CT, 2010.
[36] J.B. Foresman, in: E. Frisch (Ed.), Exploring Chemistry with Electronic Structure methods: A Guide to Using Gaussian, Gaussian Inc., Pittsburg, PA, 1996.
[37] R. Dennington, T. Keith, J. Millam, Gaussview, Version 5, Semichem Inc., Shawnee Missions, KS, 2009.
[38] J.M.L. Martin, C. Van Alsenoy, GAR2PED, A Program to obtain a Potential Energy Distribution from a Gaussian Archive Record, University of Antwerp, Belgium, 2007.
[39] L.J. Bellamy, The IR Spectra of Complex Molecules, John Wiley and Sons, New York, 1975.
[40] A. Spire, M. Barthes, H. Kallouai, G. De Nunzio, Physics D 137 (2000) 392–396.
[41] G. Socrates, Infrared Characteristic Group Frequencies, John Wiley and Sons, New York, 1981.
[42] N.P.G. Roeges, A Guide to the Complete Interpretation of IR Spectra of Organic Compounds, Wiley, New York, 1994.
[43] R. Minitha, Y.S. Mary, H.T. Varghese, C.Y. Panicker, R. Ravindran, K. Raju, V.M. Nair, J. Mol. Struct. 985 (2011) 316–322.
[44] C.Y. Panicker, H.T. Varghese, V.S. Madhavan, S. Mathew, J. Vinsova, C.V. Alsenoy, Y.S. Mary, Y.S. Mary, J. Raman Spectrosc. 40 (2009) 2176–2186.
[45] S. Kundoo, A.N. Banerjee, P. Saha, K.K. Chattophyay, Mater. Lett. 57 (2003) 2193–2197.
[46] R.T. Ulahannan, C.Y. Panicker, H.T. Varghese, C. Van Alsenoy, R. Musiol, J. Jampilek, P.L. Anto, Spectrochim. Acta A 121 (2014) 445–456.
[47] R.T. Ulahannan, C.Y. Panicker, H.T. Varghese, C. Van Alsenoy, R. Musiol, J. Jampilek, P.L. Anto, Spectrochim. Acta A 121 (2014) 404–414.
[48] K. Nakanishi, Infrared Absorption Spectroscopy Practical, Holden-Day, San Francisco, 1962.
[49] R.M. Silverstein, G.C. Bassler, T.C. Morril, Spectrometric Identification of Organic Compounds, fifth ed., John Wiley and Sons Inc., Singapore, 1991.
[50] J.B. Bhagyasree, H.T. Varghese, C.Y. Panicker, J. Samuel, C. Van Alsenoy, K. Bolelli, I. Yildiz, E. Aki, Spectrochim. Acta A 102 (2013) 99–113.
[51] T. Joseph, H.T. Varaghese, C.Y. Panicker, T. Thiemann, K. Viswanthan, C. Van Alsenoy, T.K. Manojkumar, Spectrochim. Acta A 117 (2014) 413–421.
[52] N.B. Colthup, L.H. Daly, S.E. Wiberly, Introduction to Infrared and Raman Spectroscopy, second ed., Academic Press, New York, 1975.
[53] J. Coates, in: R.A. Meyers (Ed.), Encyclopedia of Analytical Chemistry: Interpretation of Infrared Spectra: A Practical Approach, John Wiley and Sons, Chichester, 2000.
[54] M. Kaur, Y.S. Mary, H.T. Varghese, C.Y. Panicker, H.S. Yathirajan, M.S. Siddegowda, C. Van Alsenoy, Spectrochim. Acta A 98 (2012) 91–99.
[55] V.S. Madhavan, Y.S. Mary, H.T. Varghese, C.Y. Panicker, S. Mathew, C. Van Alsenoy, J. Vinsova, Spectrochim. Acta A 89 (2012) 308–316.
[56] A. Chandran, H.T. Varghese, Y.S. Mary, C.Y. Panicker, T.K. Manojkumar, C. Van Alsenoy, G. Rajendran, Spectrochim. Acta A 87 (2012) 29–39.
[57] G. Varsanyi, Assignments of Vibrational Spectra of Seven Hundred Benzene Derivatives, Wiley, New York, 1974.
[58] V.S. Madhavan, H.T. Varghese, S. Mathew, J. Vinsova, C.Y. Panicker, Spectrochim. Acta A 72 (2009) 547–553.
[59] C.Y. Panicker, H.T. Varghese, K.R. Ambujakshan, S. Mathew, S. Ganguli, A.K. Nanda, C. Van Alsenoy, Y.S. Mary, J. Mol. Struct. 963 (2010) 137–144.
[60] D.A. Kleinman, Phys. Rev. 126 (1962) 1977–1979.
[61] M. Adant, L. Dupuis, L. Bredas, Int. J. Quantum Chem. 56 (2004) 497–507.
[62] R.G. Parr, L.V. Szentpaly, S.J. Liu, J. Am. Chem. Soc. 121 (1999) 1922–1924.
[63] P.K. Chaltraj, B. Maiti, U.J. Sarbar, J. Phys. Chem. A 107 (2003) 4973–4975.

[64] R.G. Parr, R.A. Donnelly, M. Levy, W.E. Palke, J. Chem. Phys. 68 (1978) 3801–3807.
[65] R. Parthasarathi, J. Padmanabhan, V. Subramanian, B. Maiti, P.K. Chattraj, J. Phys. Chem. A 107 (2003) 10346–10352.
[66] R. Parthasarathi, V. Subramanian, D.R. Roy, P.K. Chattaraj, Bioorg. Med. Chem. 12 (2004) 5533–5553.
[67] E. Scrocco, J. Tomasi, Adv. Quantum Chem. 103 (1978) 115–121.
[68] F.J. Luque, J.M. Lopez, M. Orozco, Theor. Chem. Acc. 103 (2000) 343–345.
[69] P. Politzer, J.S. Murray, Theoretical Biochemistry and Molecular Biophysics: A Comprehensive Survey, in: D.L. Beveridge, R. Lavery (Eds.), Protein, vol. 2, Adenine Press, Schenectady, NY, 1991.
[70] E. Scrocco, J. Tomasi, Curr. Chem. 7 (1973) 95–1709.
[71] A.E. Reed, F. Weinhold, J. Chem. Phys. 78 (1983) 4066–4073.
[72] A.E. Reed, F. Weinhold, J. Chem. Phys. 83 (1985) 1736–1740.
[73] A.E. Reed, R.B. Weinstock, F. Weinhold, J. Chem. Phys. 83 (1985) 735–746.
[74] J.P. Foster, F. Wienhold, J. Am. Chem. Soc. 102 (1980) 7211–7218.
[75] J. Chocholousova, V.V. Spirko, P. Hobza, Phys. Chem. Chem. Phys. 6 (2004) 37–41.
[76] Y.S. Mary, K. Raju, I. Yildiz, O. Temiz-Arpaci, H.I.S. Nogueira, C.M. Granadeiro, C. Van Alsenoy, Spectrochim. Acta A 96 (2012) 617–625.
[77] I. Sidir, Y.G. Sidir, E. Tasal, C. Ogretir, J. Mol. Struct. 980 (2010) 230–244.
[78] E. Inkaya, M. Dincer, E. Korkusuz, I. Yildirim, J. Mol. Struct. 2013 (2012) 67–74.
[79] T. Rajamani, S. Muthu, Solid State Sci. 16 (2013) 90–101.
[80] A.F. Holleman, E. Wiberg, N. Wiberg, Lehrburch der Anorganischen Chemie, De Gruyter, Berlin, 2007.